Energy and Buildings 96 (2015) 221–235

Contents lists available at ScienceDirect

Energy and Buildings

journal homepage: www.elsevier.com/locate/enbuild

Estimation of urban temperature and humidity using a lumped parameter model coupled with an EnergyPlus model

Miguel Martin [a,*], Afshin Afshari [a], Peter R. Armstrong [a], Leslie K. Norford [b]

[a] Masdar Institute of Science and Technology, PO Box 54224, Abu Dhabi, United Arab Emirates
[b] Massachusetts Institute of Technology, 77 Massachusetts Avenue, R.5-414, Cambridge, 02139 MA, United States of America

ARTICLE INFO

Article history:
Received 1 December 2014
Received in revised form 17 February 2015
Accepted 18 February 2015
Available online 11 March 2015

Keywords:
Building energy model
Urban canopy model
Urban specific humidity
Urban temperature

ABSTRACT

In this paper, we describe a lumped thermal parameter model coupled with an EnergyPlus model used for estimating temperature and specific humidity in the near-surface urban environment. Estimations made by the model are compared to measurements obtained from data loggers installed in an urban canyon of Masdar Institute (Abu Dhabi). Based on these comparisons, we first evaluate the most likely ratios of heat released into the urban canyon by a building air handling unit and the wind tower that produces adiabatically cooled air. Next, we analyze three specific case studies to obtain a local estimate of the accuracy that is reached by the coupled scheme. To estimate its global precision, we perform a sensitivity and Monte-Carlo analysis over the most likely ratios of heat emitted by the air handling unit and the wind tower. Although validation in a dense downtown is still lacking and will be undertaken in the future, this study suggests that urban temperature and humidity can be estimated with an acceptable accuracy under moderate waste heat releases and anthropogenic heat gains.

1. Introduction

The Middle-East is well-known for its hot and humid climate. While a number of studies report interesting analyses of temperature and humidity measured within the urban canopy layer of European cities [1,2], Middle Eastern cities have seldom been investigated. For instance, the experiment by Charabi and Bakhit [3] highlights certain properties of the Urban Heat Island (UHI) effect measured in Muscat (Oman). The UHI phenomenon was also analyzed in Kuwait City (Kuwait) by Nasrallah et al. [4]. Comparing the UHI effect reported in several arid North American locations to the one measured in Kuwait City, they discovered that the position of the city, the absence of dense vegetation, and the height of buildings could enable us to mitigate the UHI effect in hot and arid environment.

Past studies have often focus on the experimental analysis of urban temperature, rarely giving in-depth consideration of humidity. Among the few studies providing equal attention to humidity, the research led by Jáuregui and Tejeda [5] showed the average diurnal cycle of specific humidity for rural, suburban, and urban areas of Mexico City. Nevertheless, their analysis is purely based on measurements and does not provide explicit guidance that can be used for including an estimation of humidity in an urban canopy model.

Urban canopy models were developed to improve the representation of urban areas in meteorological models. Several urban canopy models now in widespread use include a building energy model to more accurately represent the impact of building thermal processes on the ambient environment in the Urban Canopy Layer (UCL), the lowest layer of the Urban Boundary Layer (UBL) [6–8]. Urban canopy models can be run as stand-alone programs or, alternatively, driven by a meteorological simulation. In either mode, they are used mainly by the urban climate research community, which largely focuses on the characteristics of the urban environment and not the performance of buildings.

Building energy models allow us to approximate the indoor energy consumption in response to outdoor conditions. Building energy models are widely employed in isolated mode by consulting engineers working with architects and building owners. After defining a suitable basic design, analysts try to evaluate the efficiency of different design options or retrofitting strategies [9,10]. The main drawback in using building energy models in a stand-alone mode is that the UHI phenomenon is neglected.

* Corresponding author. Tel.: +971 28109333.
E-mail address: mmartin@masdar.ac.ae (M. Martin).

http://dx.doi.org/10.1016/j.enbuild.2015.02.047
0378-7788/

α_x	albedo of surface x, –
δ_{ex}	air handling unit exhaust heat ratio, – or %
δ_{wt}	wind tower heat ratio, – or %
ε	emissivity, –
η_q	latent heat recovery effectiveness, – or %
η_T	sensible heat recovery effectiveness, – or %
ρ_x	density of x, kg/m^3
ϕ_x	relative humidity of x, – or %
ω_x	water content of x, m^3/m^3
A_x	area of x, m^2
C_x	sensible heat capacitance of x, J/K
$\widetilde{C}_x$	latent heat capacitance of x, J
c_x	specific heat of x, J/(kg K)
d_x	depth of x, m
H_x	scheduled dependent value of x- or %
I_x	water provided by irrigation on x, kg/(m^2 s)
k	U-value, W/(m^2 K)
L_x	latent heat of vaporization of x, J/kg
l_x	length of x, m
$\dot{m}_x$	mass flow rate of x, kg/s
$n(.)$	cardinality, –
Q_x	sensible heat of x, W
$\widetilde{Q}_x$	latent heat of x, W
P_x	precipitation on x, kg/(m^2 s)
p_x	pressure on x, Pa
q_x	specific humidity of x, kg/kg
q_{sat}	specific humidity at saturation, kg/kg
$R_{x,y}$	sensible heat resistance between x and y, (m^2 K)/W
$\widetilde{R}_{x,y}$	latent heat resistance between x and y, m^2/W
$r_{x,y}$	aerodynamic resistance between x and y, s/m
T_x	temperature of x, $^\circ C$ or K
$\bar{T}_x$	average temperature of x, $^\circ C$ or K
t	time, s
V_x	volume of x, m^3
w_x	width of x, m
z_x	height of x, m

Subscripts

b	building
ex	exhaust air from the air handling unit
f	facade
g	ground (soil)
HL	HOBO logger
I	irrigation system
s	street
sky	sky
r	road
ubl	urban boundary layer
urb	urban canyon
veg	vegetation
wa	wall
wi	window
wt	wind tower

Before developing a building energy model for Town Energy Balance (TEB), Bueno et al. [11] coupled TEB to an EnergyPlus[1] model to exploit the advantages and overcome the drawbacks of both. To develop a simulation scheme of complexity appropriate for building professionals and engineers, Bueno proposed a Resistance and Capacitance (RC) representation of a building energy model and the coupled adjacent atmosphere [13]. In the Urban Weather Generator (UWG), he extended the lumped parameter approach to energy balances to include a rural reference weather station and the UBL above the UCL [14]. In this way, the UWG maps a reference weather file to estimated conditions at an urban neighborhood. While the UWG itself necessarily couples the building to the UCL, the use of the UWG is decoupled from the building energy model. This requires the user to provide to the UWG the same key building parameters to be used in the building energy model.

This paper proposes a new method that leverages the capabilities of detailed building performance simulations but retains the direct coupling of that simulation with a representation of the urban canopy model, for which the new scheme uses a lumped thermal parameter model. The fact of coupling an urban canopy model with an EnergyPlus model ordinarily adds complexity in terms of software programming. In order to solve this issue, we decided to use the Building Controls Virtual Test Bed (BCVTB) [15]. This technology allowed us to implement a Matlab thread that executes the lumped thermal parameter model and communicates with the EnergyPlus external interface. While building surface temperatures and convective heat transfer coefficients, waste heat emissions, and air handling unit exhausts approximated from the EnergyPlus model were iteratively employed by the lumped thermal parameter model, the latter was mainly in charge of computing dry-bulb temperature, wet-bulb temperature, and wind speed in the UCL to improve the accuracy of exterior surface conditions considered by the EnergyPlus model.

The coupled scheme can be used in several applications. First, a model of urban temperature is required to estimate the building cooling energy penalty due to the UHI effect. The model also allows us to develop and test different approaches to reducing the UHI effect. Finally, in order to optimize city-wide demand side management interventions, what-if retrofitting scenarios can easily be generated and evaluated by changing the parameters of the coupled scheme model. This could become an effective decision support tool for policy makers. Before being employed in all these applications, the reliability of the coupled scheme in terms of urban temperature and specific humidity estimations must be proved.

2. Coupled scheme

To estimate dry-bulb temperature and specific humidity in the UCL of Masdar Institute, we coupled a lumped thermal parameter model with an EnergyPlus model. First, the EnergyPlus model calculates sensible and latent heat fluxes coming from air handling unit exhausts, and waste heat releases. The building energy model also computes wall and window surface temperature. Next, all these values are employed by the lumped thermal parameter model to evaluate the urban canyon temperature, specific humidity, and pressure. The same parameters are also computed for road and soil surfaces. In addition to the information assessed from the EnergyPlus model, the lumped thermal parameter model requires values for meteorological parameters in the UBL: dry-bulb temperature, precipitation, pressure, relative humidity, and wind speed. For this purpose, an EnergyPlus weather file is created based on actual hourly measurements we obtained from the weather station located at the top of the Masdar wind tower. Finally, the dry-bulb temperature, wet-bulb temperature, and wind speed calculated from the lumped thermal parameter model are used by the EnergyPlus model as outdoor boundary conditions of walls and windows.

Fig. 1 shows the urban topography we considered for designing the coupled scheme. Like Bueno et al. [11], the building defined via the EnergyPlus model (also called the reference building) is assumed to be surrounded by buildings of equal height z_b, length

[1] EnergyPlus is a detailed dynamic building energy simulation engine (cf. Crawley et al. [12]).

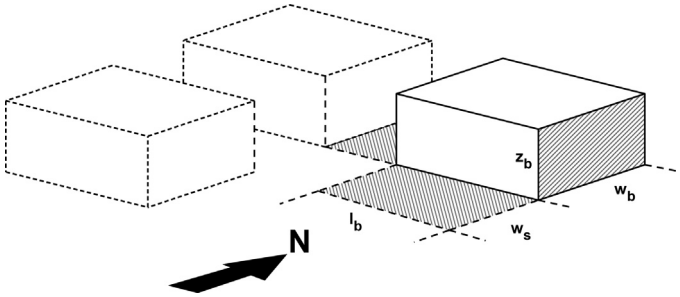

Fig. 1. 3D urban topography considered by the coupled-scheme. Buildings are assumed to have same dimensions and thermal properties. Streets are also identical.

l_b, and width w_b. Streets located all around the reference building are also the same width w_s.

Similar to Bueno et al. [13], we defined a system of differential equations representing sensible heat transfers from the UBL, streets, and buildings to the urban canyon. The resulting state space model has three state variables: urban canyon air temperature, road temperature, and ground temperature. As input variables, we included UBL temperature, left and right façade temperatures, and additional sensible heat gain Q^*_{urb}. The latter corresponds to the sum of sensible heat coming from anthropogenic activity Q_{ag} (i.e. heat releases emitted by human activity on streets), exhausts Q_{ex} (i.e. heat rejected by the air handling unit), waste heat releases Q_{wr} (i.e. heat rejected by the chiller plant), and the Masdar wind tower Q_{wt}. Even though anthropogenic heat gains and waste heat releases are negligible in Masdar Institute (i.e. $Q_{ag} \cong 0$ and $Q_{wr} \cong 0$), we decided to consider these two parameters to test the coupled scheme in a future case study in which they would be significant. The sensible heat released by the air handling unit Q_{ex} and the Masdar wind tower Q_{wt} can be computed as:

$$Q_{ex} = \delta_{ex}(Q_{ex,zones} - Q_{recov}) \tag{1}$$

$$Q_{wt} = \delta_{wt} H_{wt} \dot{m}_{wt} c_p (T_{wt} - T_{urb}) \tag{2}$$

where δ_{ex} and δ_{wt} are the ratios of heat coming from the air handling unit and the Masdar wind tower, respectively, going into the urban canyon. These two formulas are further explained in Appendices A and B. The resulting lumped parameter model is illustrated in Fig. 2.

Following a similar strategy, we expressed latent heat exchanges in terms of latent heat capacitances and latent heat resistances (cf. Fig. 3). Comparable to the system of differential equations defining sensible heat transfers, latent heat exchanges can be solved as a state space model with one state variable: the

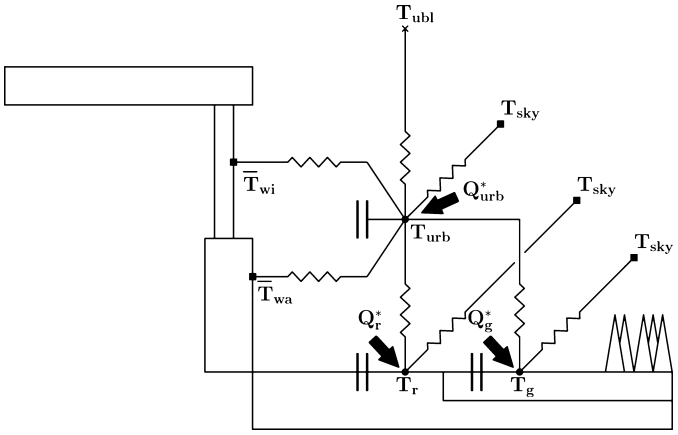

Fig. 2. Lumped thermal parameter model used for the computation of sensible heat exchanges where $Q^*_{urb} = Q_{ag} + Q_{ex} + Q_{wr} + Q_{wt}$. It shows variables that are internally computed (solid circle), and the ones obtained from the weather file (cross) and the EnergyPlus model (solid square).

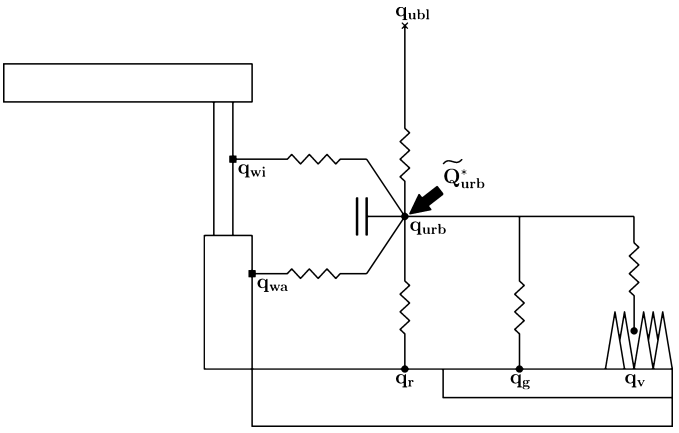

Fig. 3. Lumped thermal parameter model used for the computation of latent heat exchanges where $\widetilde{Q}^*_{urb} = \widetilde{Q}_{ag} + \widetilde{Q}_{ex} + \widetilde{Q}_{wr} + \widetilde{Q}_{wt}$. In agreement with [6,22], we defined $q_{wi} = q_{sat}(\bar{T}_{wi}, p_{urb})$, $q_{wa} = q_{sat}(\bar{T}_{wa}, p_{urb})$, $q_r = q_{sat}(T_r, p_s)$, $q_g = \phi_g q_{sat}(T_g, p_s)$, and $q_{veg} = q_{sat}(T_g, p_s)$.

urban specific humidity. The input variables are represented by specific humidity of the UBL, ground, vegetation, walls, and windows. The additional latent heat gain in the urban canyon $\widetilde{Q}^*_{urb}$ was assessed from the same source of heat as Q^*_{urb} such as:

$$\widetilde{Q}_{ex} = \delta_{ex}(\widetilde{Q}_{ex,zones} - \widetilde{Q}_{recov}) \tag{3}$$

$$\widetilde{Q}_{wt} = \delta_{wt} H_{wt} \dot{m}_{wt} L_v (q_{wt} - q_{urb}) \tag{4}$$

According to Masson [6], a latent heat resistance $\widetilde{R}_{x,urb}$ between any thermal node x and the urban canyon urb can be calculated as function of an aerodynamic resistance $r_{x,urb} = c_{urb}\rho_{urb}R_{x,urb}$:

$$\widetilde{R}_{x,urb} = \frac{r_{x,urb}}{L_{urb}\rho_{urb}} = \frac{c_{urb}}{L_{urb}} R_{x,urb} \tag{5}$$

where $R_{x,urb}$ is the sensible heat resistance. The latent heat capacitance of the urban canyon $\widetilde{C}_{urb}$ can also be expressed as a function of a sensible heat capacitance C_{urb}:

$$\widetilde{C}_{urb} = V_{urb} L_{urb} \rho_{urb} = \frac{L_{urb}}{c_{urb}} C_{urb} \tag{6}$$

While incident solar gain on street surfaces was processed by the lumped thermal model, the EnergyPlus model was in charge of computing incident solar radiations on façade surfaces. The way EnergyPlus performs incident solar radiation calculations on wall and window surfaces can be found in the Engineering Ref. [16]. Unfortunately, the only parameters one can change on wall and window surfaces via the EnergyPlus external interface are convective heat transfer coefficient, outdoor air dry-bulb temperature, outdoor air wet-bulb temperature, and outdoor air wind speed (at least in EnergyPlus v.8.1). An access to the variable managing incident solar gain on façade surfaces would be a great feature to add in future versions of EnergyPlus.

2.1. Solar radiation incident on street surfaces

The sensible heat gains on the road and the ground depend on solar radiation incident on their respective surfaces (i.e. $Q^*_r = A_r S^*_s(\alpha_r)$ and $Q^*_g = A_g S^*_s(\alpha_g)$). Based on Masson [6], solar radiation incident on surface x – covering the street – was expressed as a linear combination of street direct solar radiation $S^{\Downarrow}_s$, street diffuse solar radiation $S^{\downarrow}_s$, and solar reflection incident from façades M_f Given the albedo α_x:

$$S^*(\alpha_x) = (1-\alpha_x)S^{\Downarrow}_s + (1-\alpha_x)S^{\downarrow}_s + (1-\alpha_x)(1-\Psi_s)M_f \tag{7}$$

where Ψ_s is the sky view factor of street surface.

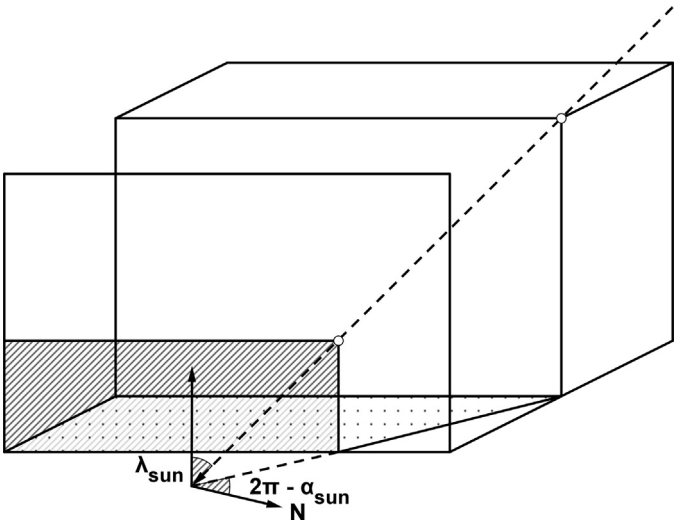

Fig. 4. Estimation of road and facade shaded area based on zenith λ_{sun} and azimuth α_{sun} angles of the sun.

In the literature, the shaded area in an urban canyon is expressed as a function of the zenith angle only [6,8]. As demonstrated in Fig. 4, we tried to improve the computation of the direct solar radiations $S_s^{\Downarrow}$ and $S_f^{\Downarrow}$ reaching the street surface and the sun exposed façade, respectively. Based on trigonometry of zenith and azimuth angles of the sun λ_{sun} and α_{sun}, respectively, we approximated the street shaded area A_s^* either as a trapezoid or as a triangle, and the façade shaded area A_f^* as a rectangle. Referring to Eq. (4.15) of Bueno Unzeta [17], we adopted the expressions for street and façade direct solar gain:

$$S_s^{\Downarrow} = I_{dir}\cos(\lambda_{sun})\left(1 - \frac{A_s^*}{A_s}\right) \tag{8}$$

$$S_f^{\Downarrow} = -I_{dir}\sin(\lambda_{sun})\cos(\alpha_{sun} - \theta_f)\left(1 - \frac{A_f^*}{A_f}\right) \tag{9}$$

where θ_f is the angle between the North axis and the normal vector of the shaded façade.

The calculation of solar reflections (cf. Eq. (17) of Masson [6]) was also improved by considering that street and building façades are made up of surfaces with differing albedo. Due to the fact that a building façade consists of walls and windows, we estimated the equivalent albedo of a façade $\bar{\alpha}_f$ as:

$$\bar{\alpha}_f = (1 - \delta_{wi})\alpha_{wa} + \delta_{wi}\alpha_{wi} \tag{10}$$

where δ_{wi} is the window area fraction. From our definition of a street surface, the albedo $\bar{\alpha}_s$ was evaluated as a linear combination of road albedo, ground albedo, and vegetation albedo.

$$\bar{\alpha}_s = (1 - \delta_g)\alpha_r + \delta_g(1 - \delta_{veg})\alpha_g + \delta_g\delta_{veg}\alpha_{veg} \tag{11}$$

where δ_g and δ_{veg} are the fraction of street covered by ground, and the fraction of ground covered by vegetation, respectively.

2.2. Sensible heat resistances

Referring to the literature, we expressed sensible heat resistances between the urban canyon and all connected thermal nodes. In accordance with Eq. (23) of Masson [6], we first estimate the sensible resistance between the road and the urban canyon as a function of the effective wind speed. The effective wind speed $U_{eff} = \sqrt{u_*^2 + U_{can}^2}$ inside the urban canyon depends on its vertical and horizontal wind components u_* and U_{can}, respectively. To approximate the friction velocity u_*, we employed the drag coefficient a^2F_m defined in Eq. (8) of Mascart et al. [18]. In short, a^2F_m can be described as function of the Richardson number between the UBL and the urban canyon, the roughness length for momentum $Z_{om} = z_b/10$ [19], and the roughness length for heat $Z_{oh} = Z_{om}/200$ [17]. We then iteratively obtained convective heat transfer coefficients for exterior wall h_{wa} and window h_{wi} surfaces employing an EnergyPlus model. We made the choice of using the Thermal Analysis Research Program (TARP) as the surface convection algorithm [20]. Consequently, we simply defined the sensible heat resistance between façade surfaces and the urban canyon as the inverse of convective heat transfer coefficient. Next, the sensible heat resistance between the UBL and the urban canyon is evaluated based on the exchange velocity U_{ex} defined in Eq. (C.13) of Bueno Unzeta [21]. In addition to heat fluxes traveling from the UBL, the street surfaces, and façade surfaces to the urban canyon, we finally consider long wave radiative heat interactions with the sky (cf. Eqs. (D.1)–(D.2) of Bueno Unzeta [21]). Estimations of the effective sky temperature T_{sky} are computed by the EnergyPlus model.

The computation of some sensible heat resistances requires the estimation of pressures inside the urban canyon. Supposing that all pressures measured at the UBL are hydrostatic, we can express the pressure at the top of an urban canyon p_{z_b} as:

$$p_{z_b} = p_{ubl} + \rho_{ubl}gz_b \tag{12}$$

where z_b and $g = 9.81\,\mathrm{m/s^2}$ are the height of the urban canyon and the gravitational acceleration, respectively. Making the same assumption for pressures in the UCL, we defined the pressure in the urban canyon p_{urb} and at street level p_s as the pressure we could measure at height $z_b/2$ and 0, respectively:

$$p_{urb} = p_{z_b} + \frac{1}{2}\rho_{urb}gz_b \tag{13}$$

$$p_s = p_{z_b} + \rho_{urb}gz_b \tag{14}$$

where ρ_{urb} is the density of the urban air canyon.

2.3. Ground relative humidity

Referring to Eqs. (11) and (12) of Noilhan and Mahfouf [22], the relative humidity of the ground ϕ_g depends on its water content ω_g. Assuming that the water coming from the deep-soil is negligible compared to water provided by precipitation and the irrigation system, the variation over time of the ground water content can be estimated as:

$$\frac{d\omega_g}{dt} = \frac{C_1}{\rho_w d_g}(\widetilde{P}_g - E_g) \tag{15}$$

where $\rho_w = 10^3\,\mathrm{kg/m^3}$ is the density of water. To include the water provided by an irrigation system, we defined ground precipitation $\widetilde{P}_g = \widetilde{P}_{ubl} + H_I I_g$ as the summation of precipitation coming from the UBL $\widetilde{P}_{ubl}$ and the effective water provided by the irrigation system $H_I I_g$ at a given hour of the day. The formula used for evaluating evaporation of water from the ground E_g was adopted from Eq. (14) of Noilhan and Mahfouf [22] using $r_{g,urb} = c_{urb}\rho_{urb}R_{g,urb}$ as the aerodynamic resistance between the ground and the urban canyon.

The force-restore coefficient C_1 should be approximated in two different ways depending on the current water content ω_g compared to the wilting point ω_{wilt}:

$$C_1 = \begin{cases} C_{1sat}\left(\dfrac{\omega_{sat}}{\omega_g}\right)^{b/2+1} & \text{If } \omega_g \geq \omega_{wilt} \\ C_{1\max}\exp\left[-\dfrac{(\omega_g - \omega_{\max})^2}{2\sigma^2}\right] & \text{otherwise} \end{cases} \tag{16}$$

Fig. 5. Masdar Institute residential buildings (left) and laboratories (right).

The first case of Eq. (16) was calculated using the formula of C_{1sat} presented by Noilhan and Planton [23], while the second was evaluated using the parameters C_{1max}, ω_{max}, and σ defined in Noilhan and Mahfouf [22].

3. Case study

Masdar Institute is a new graduate university located in Masdar City (near Abu Dhabi, UAE). The campus consists of residential and laboratory buildings. Residential buildings associate traditional regional architecture with modern technologies to satisfy demands of style as well as energy efficiency. The laboratories are made of highly insulated and air tight façades for reducing indoor cooling demand in an extremely hot environment. To limit the anthropogenic heat gain, an underground network of personal rapid transit vehicles has been installed in the undercroft of Masdar Institute. Most of buildings at Masdar Institute are equipped with a metering system to provide energy consumption to the building management system in each unit.

Both residential buildings and laboratories were designed to create a low energy cost neighborhood. The campus pedestrian streets are characterized by a relatively high height-to-width ratio and oriented to benefit from the shading effect. Each residence interior hallway has an automatically controlled and naturally ventilated central atrium cooling the interior of walls. Each atrium is connected to openings on the podium level where fresh air comes from, and louvers at the top of the building where cool air flows out. These openings are closed when the outdoor temperature is high. The metering system in each apartment enables building facilities managers and individual occupants to monitor and alter energy consumption depending on the demand in electricity, water, or cooling. To reduce the amount of heat flowing in the buildings, the envelope of laboratories is composed of highly insulated and air tight façades. A natural daylight control system is used for windows to eliminate high and low level angled sunlight. A picture of both residential and laboratory buildings is shown in Fig. 5.

To improve outdoor and indoor thermal comfort, two specific systems were installed in Masdar Institute: a district energy system providing chilled water, and air handling units providing fresh air. The central plant of the district system is located around 500 m from the campus. Therefore, waste heat releases caused by chiller have no impact on urban temperature of Masdar Institute. Cool air in residences and laboratories is delivered by four air handling units: North-East, North-West, South-East, and South-West unit. Air handling units are installed underground so as to get air at ground level and release it at roof level. Contrary to chiller waste heat, the heat rejected by air handling units through exhaust risers might have a significant impact on urban temperatures.

3.1. Wave block urban canyon

Among all urban canyons located in Masdar Institute, the one adjacent to the Wave Block was chosen as a case study for validating the coupled scheme. The street consists of sandy soil and terracotta. All around vegetation, the soil is covered by woodchips and irrigated by a system operated at night to avoid significant losses of water. The Wave Block canyon is bounded by two façades: one from a residential building (the Wave Block), and the other from a laboratory (Lab 1A Sector 01-11). Both the Wave Block and Lab 1A Sector 01-11 are connected to the North-West air handling unit. This air handling unit has a capacity of 14.2 m^3/s and employs two heat recovery wheels providing both sensible and latent recovery.

4. Validation environment

4.1. Experimental network

To measure the urban temperature and relative humidity in Masdar Institute, a network of 72 HOBO loggers (Onset U12) was installed, 18 at each of four heights: 3, 7, 11, and 15 m above street level. These devices measured dry-bulb temperature and relative humidity at a sampling rate of 15 min. Fig. 6 shows the location of each HOBO logger in the campus. For validation, we initially wanted to use eight HOBO loggers installed in the Wave Block canyon. During the period of measurement, we lost two loggers, one at 11 and the other at 15 m. This means that dry-bulb temperature and relative humidity were finally measured between August 14th and October 3rd 2011 by six HOBO loggers in the Wave Block canyon.

Weather conditions in the UBL above Masdar Institute were measured by a meteorological station installed at the top of the wind tower, 45 m above the street level. The Masdar Wind Tower Weather Station is equipped with one temperature and relative humidity probe (Vaisala HMP45C), one ultrasonic anemometer (RM Young 85000), one barometric pressure sensor (RM Young 61302V), and one tipping bucket rain gage (Texas Electronics TE525M). Direct Normal Irradiance (DNI) and Diffuse Horizontal Irradiance (DHI) measurements were obtained from a 2G and 3G, respectively, rotating shadowband pyranometer located one kilometer South of the campus.

To collect open desert conditions, a meteorological station called the Masdar Field Station was installed 700 m away from the campus. The latter measures dry-bulb temperature and relative humidity at 2 and 10 m from the ground with two probes (Vaisala HMP60). Wind speed is also recorded at two different heights – 5 and 10 m – with a 3-cup anemometer (Met One 014A) and a wind monitor (Met One 034B), respectively. The barometric pressure is measured at 1 m from the ground with a barometric sensor (Vaisala CS106).

After measuring temperature and relative humidity with HOBO loggers, the Masdar Wind Tower Weather Station, and the Masdar Field Station, we verified the reliability of measurements by detecting outliers and comparing the data with published data from field research in other urban area. Outliers were detected by applying a Hampel filter to raw measurements with an adaptive threshold of 0.1 [24]. However, it is important to clarify that detected outliers were not removed from raw measurements. This filtering procedure was only used to evaluate the percentage of outliers that might appear in measurements. Fig. 7 reveals the outliers that were detected from measurements collected from the Masdar Wind Tower Weather Station, the Masdar Field Station, and the six HOBO loggers in the canyon. To obtain an idea of the proximity of

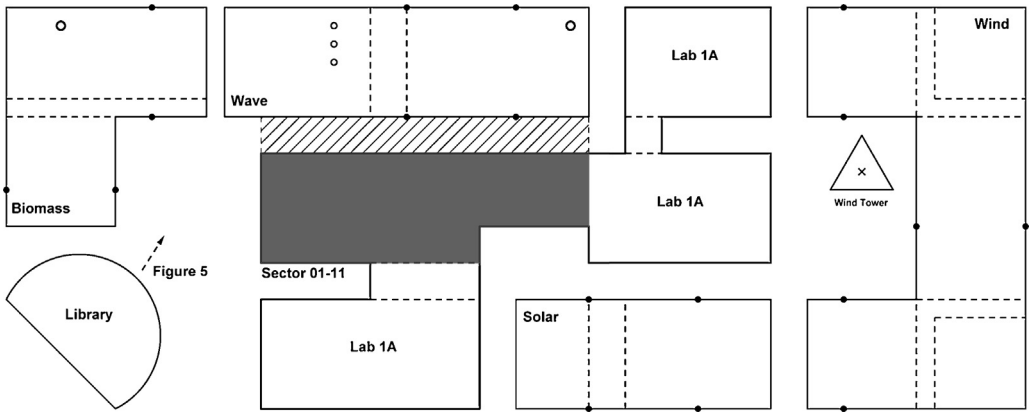

Fig. 6. Experimental network of HOBO loggers (solid circle) used for measuring urban temperature and relative humidity at Masdar Institute. The hashed area between the Wave Block and the Lab 1A Sector 01-11 corresponds to the Wave Block canyon. The location of exhaust risers connected to the North-West AHU are represented by symbol (circle). A weather station was installed at the top of the wind tower (cross) to measure meteorological conditions at the UBL.

measurements made by one HOBO logger to the others, we computed the Root Mean Square Error (RMSE) and the Mean Absolute Percentage Error (MAPE) between measurements recorded by the given HOBO and the average of the five remaining. The same procedure was applied between the temperature and relative humidity recorded by six HOBO loggers and the ones collected either by UBL and rural station. Table 1 illustrates the percentage of outliers detected, the RMSE, and the MAPE we obtain for each HOBO loggers installed in the Wave Block canyon, the Masdar Wind Towe Weather Station, and the Masdar Field Station. In this table, it is possible to notice that all HOBO loggers are in good agreement for both temperature and relative humidity. On the other hand, measurements obtained from the Masdar Wind Tower Weather Station and the Masdar Field Station are significantly different from the

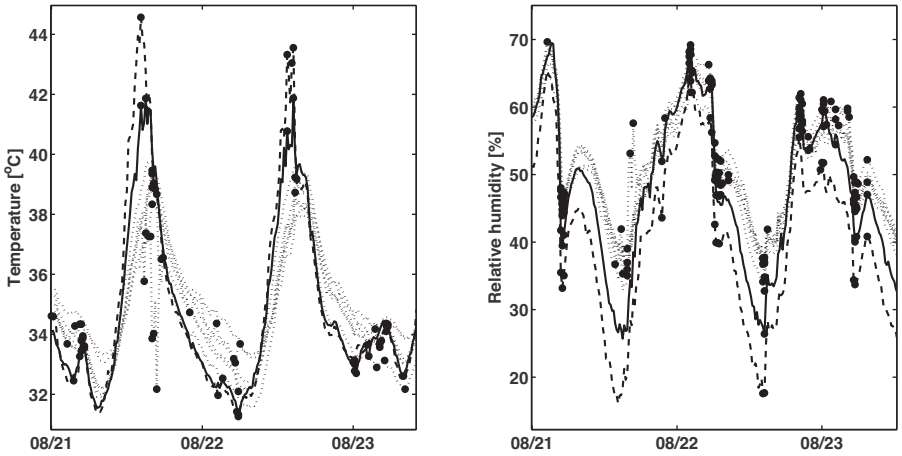

Fig. 7. Dry-bulb temperature and relative humidity measured by the Masdar Field Station (solid), the Masdar Wind Tower Weather Station (dashed), and the 6 HOBO loggers in the Wave Block canyon (dotted) with detected outliers (solid circle) between August 21st and 23rd 2011.

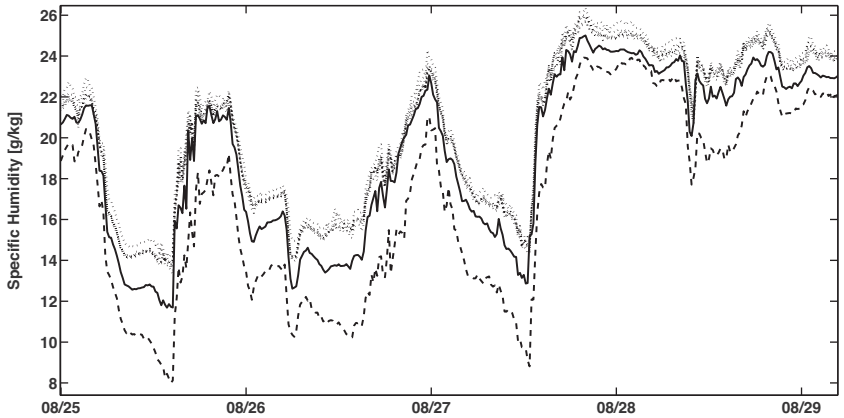

Fig. 8. Specific humidity measured by the Masdar Field Station (solid), the Masdar Wind Tower Weather Station (dashed), and the 6 HOBO loggers in the Wave Block canyon (dotted) between August 25th and 29th 2011.

Table 1
Percentage of detected outliers (PDO), root mean square error (RMSE), and mean absolute percentage error (MAPE) computed on HOBO loggers, Masdar Field Station (MFS), and Masdar Wind Tower Weather Station (MWTWS) measurements of temperature and relativity humidity between August 14th and October 3rd 2011,

	Temperature			Relative humidity		
	PDO	RMSE	MAPE	PDO	RMSE	MAPE
L0ETISALATi (3 m)	1.92	0.83	2.04	10.63	3.1	4.04
L0WAVEGATEi (3 m)	4.84	0.73	1.52	10.86	2.77	3.92
WA101 (7 m)	1.25	0.55	1.42	8.36	2	2.97
WA105 (7 m)	1.02	0.58	1.25	7.65	1.98	2.85
WA203 (11 m)	0.7	0.35	0.79	7.15	1.45	2.14
WA307 (14 m)	1.46	0.89	1.81	6.71	2.57	3.87
MWTWS	4.2	2.14	4.69	7.33	10.58	17.62
MFS	3	1.99	4.7	6.71	6.38	9.55

ones collected from HOBO loggers. This proves that raw measurements obtained from the six active HOBO loggers in the Wave Block canyon can be reliably used for analyzing urban temperature and relative humidity.

With the aim of assessing the suitability of our measurements, we compared the accuracy of our devices to the ones used to create three other datasets broadly used among the community of meteorologists for validating their statistical models. First, we compared our measurements to the BUBBLE dataset elaborated by Rotach et al. [2] which reports a wide list of measurements in selected urban canyons of Basel, Switzerland. For instance, the Sperrstrasse canyon was intensely monitored during this experimental campaign with measurements of temperature, humidity, wind, solar radiation, and gas emissions at six different heights. Next, we referred to the CAPITOUL dataset for evaluating the quality of our measurements. During this experiment led by Masson et al. [1], measurements were taken inside two urban canyons located at the intersection of Alsace-Lorraine and Pomme road (Toulouse, France). Even though good quality measurement devices were used for this experiment, urban temperature and humidity were only recorded at one point on the top of each urban canyon. We finally considered the weather dataset created by Chow and Roth [25] based on measurements taken in urban areas of Singapore. The comparison between BUBBLE, CAPITOUL, Singapore, and Masdar datasets in terms of measurement accuracy is detailed in Table 2.

Table 2
Uncertainty of Masdar Institute measurements compared to uncertainties of BUBBLE, CAPITOUL, and Singapore measurements.

	BUBBLE	CAPITOUL	Singapore	Masdar
UCL measurements				
Number of sensors/loggers (per urban canyon)	6	1	1	6
Temperature uncertainty (in °C)	±0.3	±0.3	±0.3	±0.35
Relative humidity absolute uncertainty (in %)	±1	±2	±2	±2.5
UBL measurements				
Temperature uncertainty (in °C)	±0.3	±0.1	±0.3	±0.35
Relative humidity absolute uncertainty (in %)	±1	±2	±2	±3
Wind speed uncertainty (in %)	±1	±1	±1.1	±2
Wind direction uncertainty (in °)	±1	±1	±4	±2
Pressure uncertainty (in *Pa*)	±40	–	–	±30
Precipitation uncertainty (in %)	–	±1	±2	±1
DNI uncertainty (%)	–	–	–	±4.1
DHI uncertainty (%)	–	–	–	±6.5
Rural measurements				
Temperature uncertainty (in °C)	±0.3	±0.4	±0.4	±0.6

Table 3
Characteristics of Wave Block and Lab 1A Sector 01-11 used for developing the simplified EnergyPlus model.

	Wave block	Lab 1A Sector 01-11	Average
Height	18	18	18
Width	49	40	44.5
Length	16	21	18.5
Glazing ratio (%)			
Level 0	19	35	27
Level 1	14	15	14.5
Level 2	14	15	14.5
Level 3	14	14.5	14.25
Total	15.25	19.9	17.57
U-values (W/(m^2 K))			
Wall	0.24	0.26	0.25
Windows	2.2	2.2	2.2
Wall albedo	0.2	0.4	0.3

4.2. Measured specific humidity

Fig. 8 reveals the specific humidity assessed from measurements of the Masdar Wind Tower Weather Station and the six HOBO loggers in the Wave Block canyon. As mentioned before, HOBO loggers only measure temperature and relative humidity. We computed the specific humidity from these two measurements with the following formula [26]:

$$q = 0.662 \frac{\phi_{HL} \epsilon_{sat}(T_{HL})}{p(z_{HL}) - 0.378 \phi_{HL} \epsilon_{sat}(T_{HL})} \quad (17)$$

where $p(z_{HL}) = p_{ubl} p_0(z_{HL})/p_0(z_{ubl})$ is the standard atmosphere formula for pressure computation. In Fig. 8, we can see the computed specific humidity for the six HOBO loggers in the Wave Block canyon.

4.3. EnergyPlus model

As a reference building of the coupled scheme, we implemented one simplified EnergyPlus model from average dimensions and thermal properties of two detailed EnergyPlus models: one for the Wave Block and one for the Lab 1A Sector 01-11 (cf. Table 3). The two detailed EnergyPlus models were created based on information collected from different sources. For instance, the outdoor air mass flow rate and heat recovery effectiveness of air handling units were obtained from the Masdar building management system. Albedo of walls and pavement was measured with a spectroradiometer (Apogee PS300 with AS-003 and AS-004 accessories). We referred to an internal report for the *U*-values of wall and windows surfaces. Table 3 illustrates properties and dimensions of detailed EnergyPlus models for the Wave Block and the Lab 1A Sector 01-11.

Recently, an energy monitoring system has been installed at Masdar Institute. Since June 2014, we have collected data of energy consumption in both the Wave Block and the Lab 1A Sector 01-11. The cooling energy consumption between July and October 2014 was used for calibrating detailed EnergyPlus models of these two buildings. Regarding the Lab 1A Sector 01-11 consumption, we divided the monthly cooling energy by four assuming that it is equally distributed over all sectors of Lab 1A. The results of calibration of detailed EnergyPlus models are illustrated in Fig. 9. Both Wave Block and Lab 1A Sector 01-11 EnergyPlus models were calibrated to an accuracy below 10% MAPE using actual weather data measured by the Wind Tower Weather Station during the corresponding period.

Fig. 10 shows the average diurnal cycle of exhaust sensible and latent heat fluxes as estimated by the simplified EnergyPlus model. The latter is compared to the average diurnal cycle of exhausts calculated as the mean of the diurnal cycles from the detailed

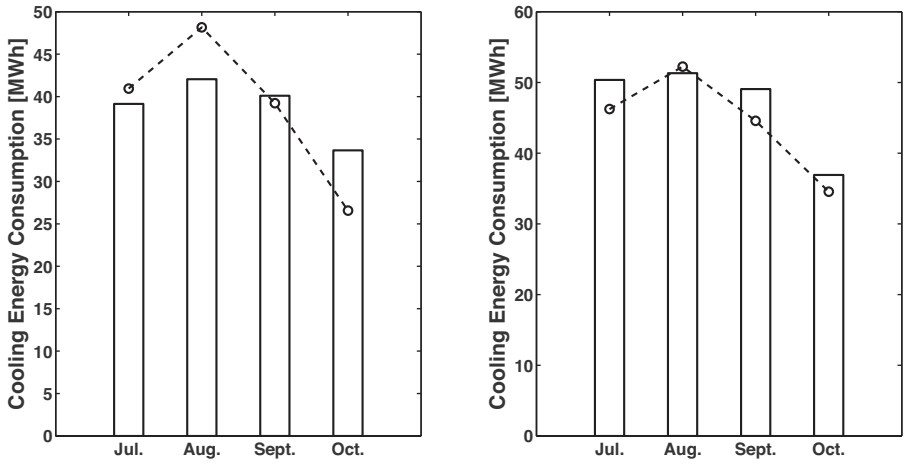

Fig. 9. Measured cooling energy consumption (bars) compared to the one estimated (dashed) from the detailed EnergyPlus model of the Wave Block (left) and Lab 1A Sector 01-11 (right).

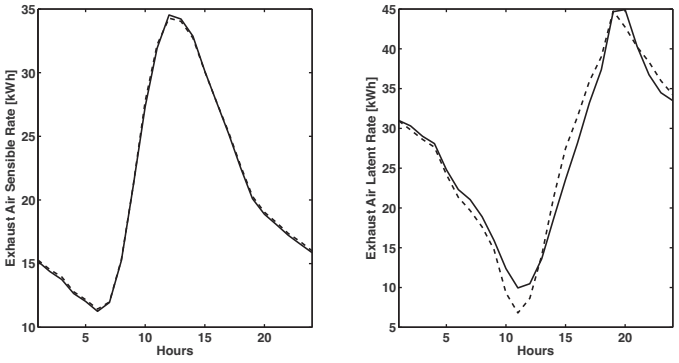

Fig. 10. Comparison between sensible and latent heat rates coming from exhausts air approximated by the simplified EnergyPlus model (dashed) and the average ones estimated by the detailed EnergyPlus models of Wave Block and Lab. 1A (solid).

EnergyPlus models for the Wave Block and Lab 1A Sector 01-11. After making a few adjustments in the simplified EnergyPlus model, we reached an accuracy of 0.8% and 7.5% MAPE in the approximation of the average diurnal cycle of sensible and latent exhausts, respectively, assessed from detailed EnergyPlus models. A representation of the simplified EnergyPlus model is shown in Fig. 11.

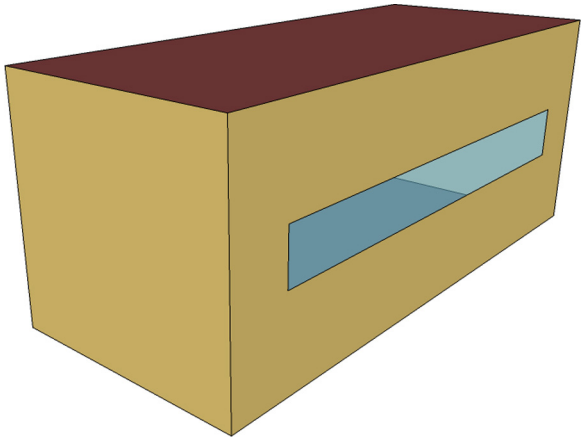

Fig. 11. Representation of simplified building used for validation of the coupled-scheme.

4.4. Invariant parameters of the coupled scheme

In addition to characteristics of the reference building (i.e. the simplified EnergyPlus model), the coupled scheme also requires some information regarding the street surface. For example, the road-to-ground and the ground-to-vegetation ratios are among the invariant parameters that the developed coupled scheme requires for running a simulation. They were computed by measuring the total surface area of ground and vegetation that covers the Wave Block canyon. Because the ground soil is entirely sand, we took the values mentioned in McCumber and Pielke [27] to defined water content parameters. Precipitation coming from the irrigation system was estimated by simulation of the water content in the Wave Block canyon. Table 4 summarizes all invariant parameters we used for estimating temperature and specific humidity in the Wave Block canyon with the coupled scheme.

Table 4
Coupled-scheme parameters we used for estimating urban temperature and specific humidity in the Wave Block canyon.

Location	Masdar City (Latitude: 24.43°; Longitude: 54.61°)
Simulation time-step	3600 s
Simulation period	05/29 – 12/31 (2011)
Street	
Width	8 m
Road	$d = 0.75$ m; $\rho c_p = 1.4 \times 10^6$ J/(m^3 K);
(= 89% of street area)	$\alpha = 0.4$; $\varepsilon = 0.95$
Ground soil	$d = 0.5$ m; $\rho c_p = 1.2 \times 10^6$ J/(m^3 K);
(= 11% of street area)	$\alpha = 0.1$; $\varepsilon = 0.8$
	Water content (Sand) - $\omega_{sat} = 0.395$ m^3/m^3;
	$\psi_{sat} = -0.121$ m; $K_{sat} = 1.76 \times 10^{-4}$ m/s; $b = 4.03$
	Vegetation (= 50% of ground surface) - $\alpha = 0.15$
Irrigation system	$I_g = 1.5 \times 10^{-3}$ kg/(m^2 s)
(Schedule: nighttime)	
Reference building	
Height	18 m
Length	18.5 m
Width	44.5 m
Number of floors	1 (i.e. 4 floors treated as one)
Orientation from North	37°
Walls	$\alpha = 0.3$; $k = 0.25$ W/(m^2 K)
West and East windows	$\alpha = 0.08$; $k = 2.2$ W/(m^2 K)
(= 17.5% of facade area)	
Thermostat	24 °C
Ideal cooling system	$\dot{m}_{inv} = 4$ m^3/s; $\eta_T = 41\%$; $\eta_q = 18\%$
(Schedule: always on)	

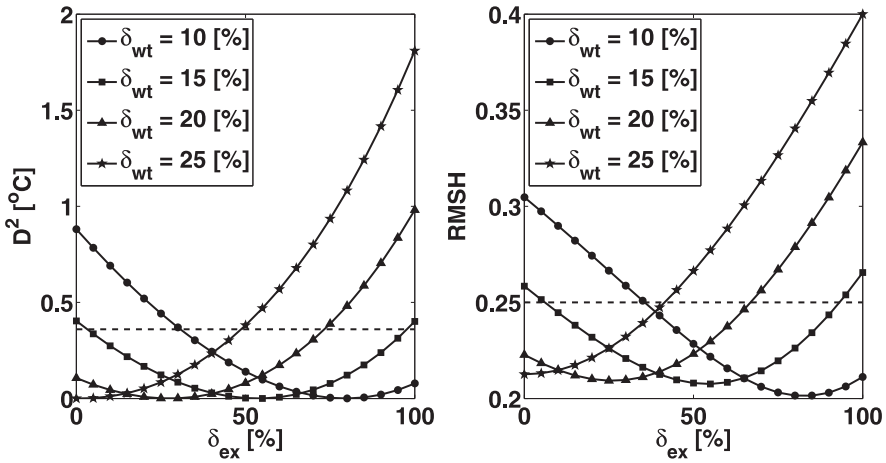

Fig. 12. Squared deviation (left) and RMSH (right) for urban temperature estimations from August 14th 2011 at 1:00 am to October 3rd at 12:00 am UTC +4 as function of exhaust and wind tower air ratios.

5. Results

The average diurnal cycle $\bar{D}_{\mathbf{x}}$ of time series $\mathbf{x} = \{x_t\}_{t=1}^{T}$ may be represented by the set of average values $\mu_h(\mathbf{x})$ and the standard deviations $\sigma_h(\mathbf{x})$ at each hour h of a day, i.e:

$$\bar{D}_{\mathbf{x}} = \{< \mu_h(\mathbf{x}), \sigma_h(\mathbf{x}) > \forall h \in \{1, \ldots, 24\}\} \tag{18}$$

$$\mu_h(\mathbf{x}) = \frac{1}{n(\mathcal{X}_h)} \sum_{x_h \in \mathcal{X}_h} x_h \tag{19}$$

$$\sigma_h(\mathbf{x}) = \sqrt{\frac{1}{n(\mathcal{X}_h)} \sum_{x_h \in \mathcal{X}_h} (x_h - \mu_h(\mathbf{x}))^2} \tag{20}$$

where $\mathcal{X}_h$ is the set of values of $\mathbf{x}$ at hour h. In this study, we developed a distance between two average diurnal cycles based on the metric of Hellinger [28]. The Hellinger distance for normal distributions is very convenient because it is defined in terms of the mean and the standard deviation. To express a distance between the averaged diurnal cycles $\bar{D}_{\mathbf{x}}$ and $\bar{D}_{\mathbf{y}}$, we computed the Root Mean Square error of Hellinger (RMSH) distances $H_h^2(\mathbf{x}, \mathbf{y})$ at each hour h:

$$RMSH(\bar{D}_{\mathbf{x}}, \bar{D}_{\mathbf{y}}) = \sqrt{\frac{1}{24} \sum_{h=1}^{24} H_h^2(\mathbf{x}, \mathbf{y})} \tag{21}$$

$$H_h^2(\mathbf{x}, \mathbf{y}) = 1 - \sqrt{\frac{2\sigma_h(\mathbf{x})\sigma_h(\mathbf{y})}{\sigma_h^2(\mathbf{x}) + \sigma_h^2(\mathbf{y})}} \times e^{-}1/4(\mu_h(\mathbf{x}) - \mu_h(\mathbf{y}))^2 / \sigma_h^2(\mathbf{x}) + \sigma_h^2(\mathbf{y}) \tag{22}$$

5.1. Likelihood of heat ratios

The accuracy of urban temperature and specific humidity estimations was computed over exhaust heat ratios δ_{ex} between 0% and 200%, and wind tower heat ratios δ_{wt} between 0% and 100%. The upper bound of 200% for the exhaust heat ratio δ_{ex} corresponds to the theoretical limit when all the heat released by the air handling unit through exhaust risers comes from both the right and the left building of the urban canyon. In practice, the two ratios δ_{ex} and δ_{wt} are difficult to measure. For this reason, we first decided to calculate the mean value and the average diurnal cycle of estimated urban temperature and specific humidity over the widest theoretical range of δ_{wt} and δ_{ex}. Then, we fixed a threshold of tolerance for the squared deviation between measured and estimated average temperature and specific humidity over the period of study. A threshold of tolerance was also defined for the RMSH between measured and approximated average diurnal cycles. Finally, we defined *the most likely range of heat ratios* as the restricted range of δ_{wt} and δ_{ex} under which urban temperature and specific humidity estimated by the coupled scheme satisfies the thresholds of tolerance.

According to the U.S. EPA [29], the peak demand for urban electricity rises between 1.5% and 2% for every 0.6 °C increase of the average outdoor temperature. Due to the fact that the interest in using a coupled scheme is also to provide an accurate approximation of the energy consumption in a building, we considered the value of 0.36 °C as threshold of tolerance for the Squared Deviation (D^2) between the measured and the estimated average urban temperature over the period of study. The value of 0.25 has been empirically chosen as threshold of the tolerance for the estimated average diurnal cycles of urban temperature.

Fig. 12 shows the D^2 between the measured and the estimated average urban temperature over the period of study. This figure also illustrates the RMSH between average diurnal cycles for urban temperature assessed from the coupled scheme and measurements. According to these two metrics, the estimated urban temperatures do not satisfy the threshold of tolerance for all values of δ_{wt} lower than 10% and higher than 25%. To achieve the threshold of tolerance for both D^2 and *RMSH* when δ_{wt} varies between 10% and 25%, δ_{ex} must be between 35% and 40% (Fig. 13).

After computing the accuracy of estimated urban temperature in terms of D^2 and RMSH over several values of δ_{ex} and δ_{wt}, we performed the same analysis with the specific humidity. As a threshold of tolerance for D^2 between the measured and the estimated average urban specific humidity, we took the value of 3 mg/kg. According to Ihara et al. [30], the sensitivity of electricity consumption to specific humidity is between 0.6 and 0.9 W/(m² g/kg). Consequently, the threshold of tolerance we chose for specific humidity potentially allows us to limit the estimation error in electricity consumption to 1.53 W/m². Regarding the RMSH between measured and estimated average diurnal cycle for specific humidity, we employed the same tolerance threshold we defined for temperature.

As illustrated in Fig. 13, estimated urban specific humidity by the coupled scheme satisfies thresholds of tolerance for D^2 and *RMSH* for all δ_{ex} lower than 45% and δ_{wt} between 10% and 25%. Based on this outcome and the previous ones, we conclude that the most likely range of heat ratios according to the coupled scheme is

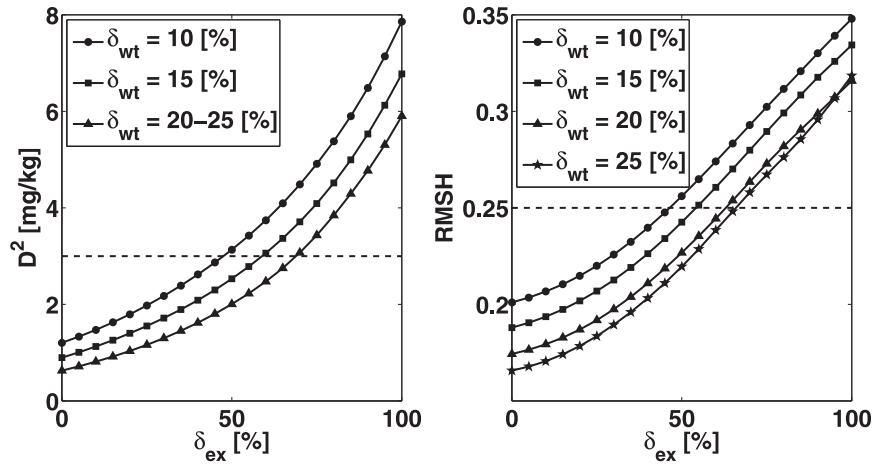

Fig. 13. Squared deviation (left) and RMSH (right) for urban specific humidity estimations from August 14th 2011 at 1:00 am to October 3rd at 12:00 am UTC +4 as function of exhaust and wind tower air ratios. It is important to note that curve representing D^2 for δ_{wt} = 20% is extremly close to the one for δ_{wt} = 25%. For this reason, we joined these two curves in one.

Table 5
Case study description for frequency distribution and average diurnal cycle analysis within the most likely range of exhaust and wind tower heat ratios.

Parameter	Case 1	Case 2	Case 3
Wind tower air ratio (%)	10	17.5	25
Exhaust air ratio (%)	40	37.5	35

expressed by values of δ_{ex} between 35% and 40%, and δ_{wt} between 10% and 25%.

5.2. Local analysis of the coupled scheme accuracy

To visualize the accuracy that can be reached by the coupled scheme at some points of the most likely range of heat ratios, we analyzed three additional cases in terms of frequency distribution and average diurnal cycle of urban temperature, urban specific humidity, and UHI intensity. Conforming to our experimental network, we defined the UHI intensity as temperature differences between HOBO loggers and the Masdar Field Station at 10 m. The first case consisted of the same configuration introduced in Table 5 with a low value of δ_{wt} and a high value of δ_{ex} in the range of most likely heat ratios. As a second case, we analyzed frequency distribution and average diurnal cycle with likely central values of δ_{wt} and δ_{ex}. The last case analyzed the accuracy that can be reached by the coupled scheme with a likely high δ_{wt} and low δ_{ex}.

All frequency distributions were computed with a normal kernel estimator of 100 points. We used the Kolmogorov–Smirnov (K–S) distance [31], a metric commonly used for computing the distance between two non-parametric distributions, to quantify the similarity of two frequency distributions. Figs. 14 and 15 illustrates the frequency distributions of urban temperature, urban specific humidity, and UHI intensity we obtained from measurements and estimations. All frequency distributions assessed from the coupled scheme seem to have a peak value well aligned with the one of frequency distributions evaluated from measurements. The variance estimation of the distributions also showed good agreement. Table 6 illustrates the K–S distance between measured and estimated frequency distributions in the three case studies.

In Figs. 16 and 17, the average diurnal cycles for urban temperature, urban specific humidity, and UHI intensity in cases 1, 2, and 3 are compared to the ones obtained from measurements. Between 10 am and 12 pm, a slight overestimation of temperature, specific humidity, and UHI intensity is evident. Even though specific humidities in the Wave Block canyon are generally underestimated by the coupled scheme, the average RMSH of

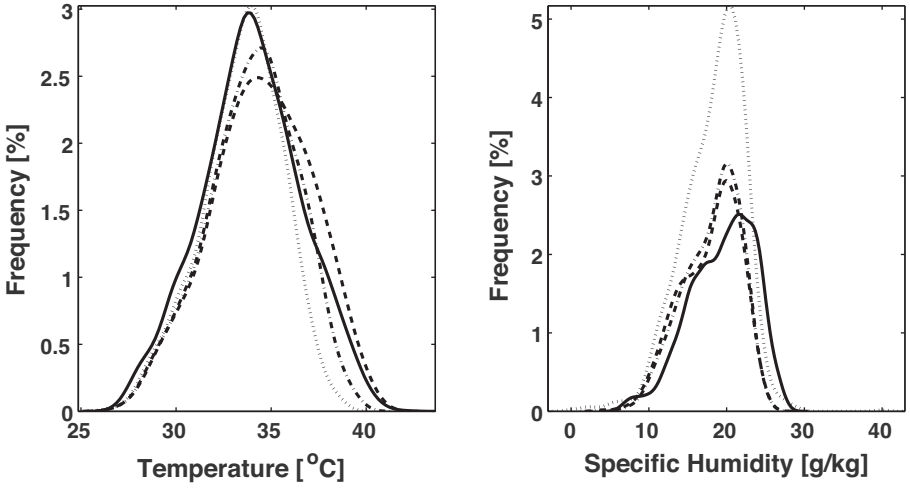

Fig. 14. Frequency distribution for dry-bulb temperature and specific humidity in the Wave Block canyon evaluated from measurements (solid), Case 1 (dashed), Case 2 (dotted and dashed), and Case 3 (dotted) between August 14th 2011 at 1:00 am and October 3rd at 12:00 am UTC +4.

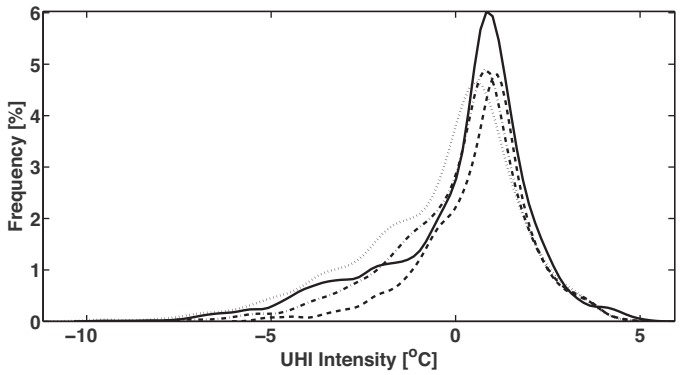

Fig. 15. Frequency distribution for UHI intensity in the Wave Block canyon evaluated from measurements (solid), Case 1 (dashed), Case 2 (dotted and dashed), and Case 3 (dotted) between August 14th 2011 at 1:00 am and October 3rd at 12:00 am UTC +4.

estimated average diurnal cycles over the three cases is about the same as that obtained for temperature and UHI intensity. As a final observation, we note that more that 95% of estimated average hourly temperatures and specific humidities are within the interval of measured standard deviations from hourly average urban conditions. This outcome drops to 83% for UHI intensity estimations in the three cases.

Table 6
K–S distance and root mean square of Hellinger distances (RMSH) for urban temperature, urban specific humidity, and UHI intensity in the three case studies.

	Case 1		Case 2		Case 3	
	K–S	RMSH	K–S	RMSH	K–S	RMSH
Temperature	23.45	0.24	25.45	0.21	33.10	0.24
Specific humidity	34.48	0.24	37.52	0.21	121.35	0.20
UHI intensity	69.68	0.26	27.74	0.23	31.43	0.34

5.3. Sensitivity and Monte-Carlo analysis

To have a global evaluation of the coupled scheme accuracy within the most likely range of exhaust and wind tower heat ratios, we decided to proceed to a sensitivity and Monte-Carlo analysis of the K–S distance and RMSH for both temperature and specific humidity. The basic procedure for sensitivity analysis aimed at computing the absolute coefficient $\Delta y_i/\Delta x_j$ of one output $y_i = f(x_1, x_2, \ldots, x_N)$ we wanted to analyze over one input x_j. The coefficient of sensitivity $\Delta y_i/\Delta x_j$ such as $\Delta y_i = f(x_1, \ldots, x_j + \Delta x_j, \ldots, x_N) - - f(x_1, \ldots, x_j, \ldots, x_N)$ was calculated over 500 uniformly generated samples of x_j with constant Δx_j. In addition to computation of sensitivity

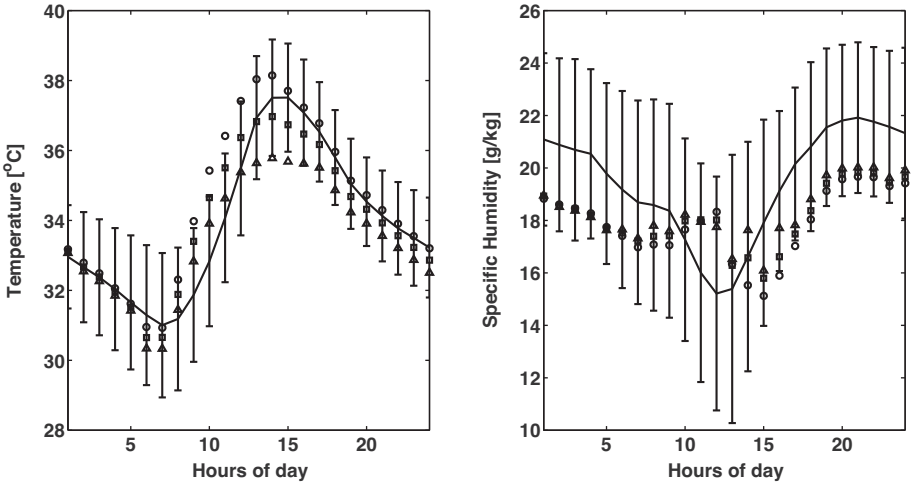

Fig. 16. Average diurnal cycles for temperature (left) and specific humidity (right) in the Wave Block canyon evaluated from measurements (solid), Case 1 (circle), Case 2 (square), and Case 3 (triangle) between August 14th 2011 at 1:00 am and October 3rd at 12:00 am UTC +4.

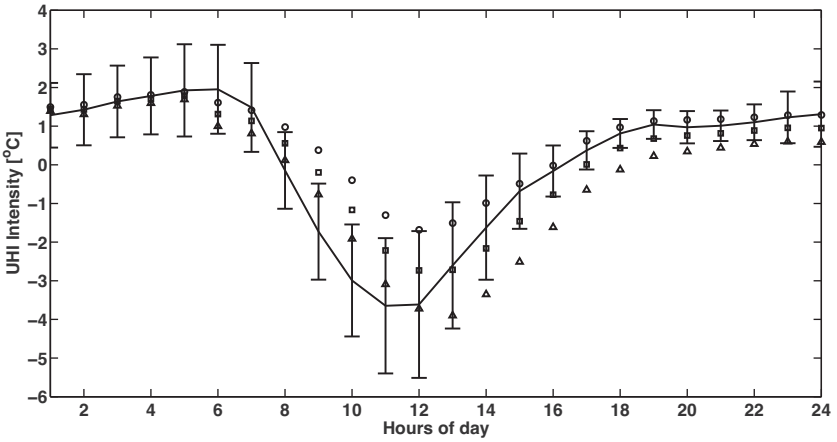

Fig. 17. Average diurnal cycles for UHI intensity in the Wave Block canyon evaluated from measurements (solid), Case 1 (circle), Case 2 (square), and Case 3 (triangle) between August 14th 2011 at 1:00 am and October 3rd at 12:00 am UTC +4.

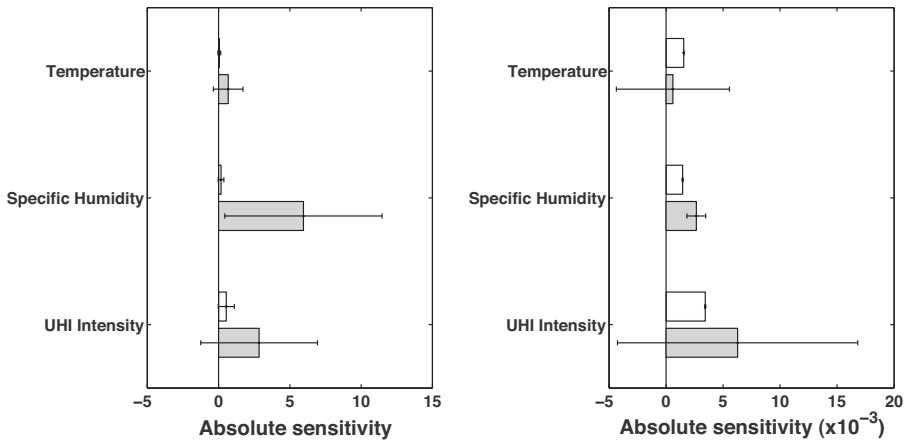

Fig. 18. Sensitivity analysis on the K-S distance (left) and the RMSH (right) with $\Delta\delta_{ex} = 1\%$ (white) and $\Delta\delta_{wt} = 1\%$ (gray).

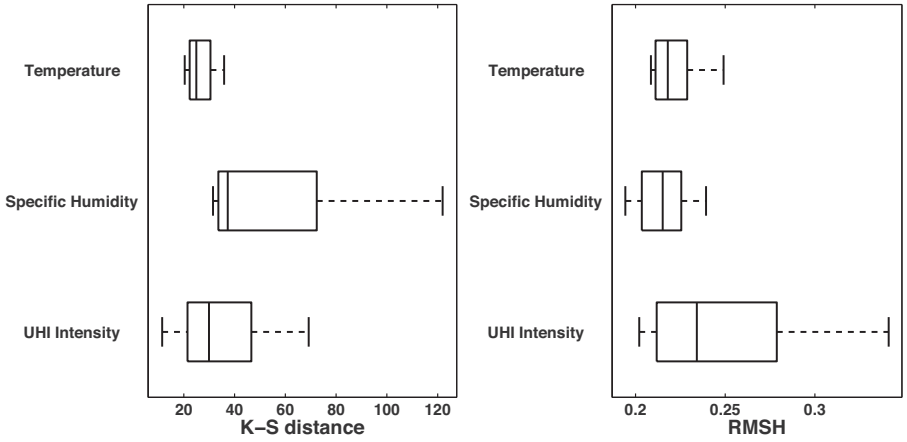

Fig. 19. Monte-Carlo analysis on the K–S distance (left) and the RMSH (right) with $\Delta\delta_{ex} \sim \mathcal{U}(35, 40)$ and $\Delta\delta_{wt} \sim \mathcal{U}(10, 25)$.

coefficients, we finally estimated the frequency distribution of each output $y_i = f(\mathbf{x})$ based on 1200 uniformly generated inputs $\mathbf{x} = [x_1, \ldots, x_N]$.

Fig. 18 shows the mean and the standard deviation of absolute sensitivity coefficients computed from the K-S distance and RMSH of urban temperature, urban specific humidity, and UHI intensity approximations over the most likely values of δ_{ex} and δ_{wt}. The first observation we can make is that the accuracy of the coupled scheme responses are more sensitive to δ_{wt} than δ_{ex}. While the accuracy with which the coupled scheme estimates urban specific humidity has the highest sensitivity in terms of frequency distribution, the UHI intensity approximations show the strongest sensitivity for the precision of average diurnal cycles.

Fig. 19 illustrates the Monte-Carlo analysis we performed on the accuracy with which the coupled-scheme evaluates urban temperature, urban specific humidity, and UHI intensity in the Wave Block canyon. While the precision of specific humidity has the highest variance in terms of K–S distance, the highest degree of unpredictability for the RMSH is reached by estimations of UHI intensity.

6. Conclusion

In this study, we have presented a lumped parameter urban canopy model coupled with an EnergyPlus model. The coupled scheme was used to estimate urban temperature and humidity inside an urban canyon at Masdar Institute (Abu Dhabi). The developed urban canopy model took into consideration heat fluxes coming from the urban boundary layer, the sky, walls, windows, road, ground, vegetations, the air handling unit, and the Masdar wind tower.

To assess the accuracy of the coupled scheme, we first estimated the urban temperature and humidity over the theoretical range of ratios of heat coming from the air handling unit and the wind tower. For each estimation, we computed the squared deviation and the root mean square error of Hellinger of two-month and hourly average values, respectively. Then, we calculated the frequency distributions and the average diurnal cycles of urban temperature, of urban specific humidity, and of UHI intensity estimated from three test cases selected within the most likely range of exhaust and wind tower heat ratios. Finally, we performed a sensitivity and Monte-Carlo analysis on the accuracy with which the coupled scheme approximates the frequency distribution and the average diurnal cycle of these three urban micro-climate parameters over uniformly chosen ratios of exhaust and wind tower heat within the most likely range.

Considering 0.36 °C and 3 mg of water per kilogram as threshold of tolerance for the D^2 of estimated average urban temperature and specific humidity, respectively, and 0.25 as threshold for the RMSH of both urban conditions, we found that the most likely range of exhaust heat ratio is between 35% and 40% when the wind tower heat ratio is between 10% and 25%. Based on the three cases, we observed that the frequency distribution and the average diurnal

cycle of temperature, specific humidity, and UHI intensity in the Wave Block canyon can be closely approximated by the coupled scheme, although small divergences appears between 10 am and 12 pm in diurnal cycles. The study also shows that, in terms of both sensitivity and Monte-Carlo analysis, estimations of urban specific humidity are the least accurate in terms of frequency distribution. According to both sensitivity and Monte-Carlo analysis, the least precise urban parameter approximated by the coupled-scheme in terms of average diurnal cycle is the UHI intensity.

Several future works are envisaged to extend this study. First, it may be worthwhile to develop an embedded building energy model into the lumped thermal urban canopy model. The use of EnergyPlus with BCVTB may be disadvantageous when we want to change a time dependent variable that is not available through the external interface; like solar radiation incident on walls and windows. Furthermore, the amount of parameters we have to specify in an EnergyPlus model is larger than what needed to compute with acceptable accuracy the thermal interactions between a building and the adjacent outdoor environment. The fact that the coupled scheme proved to be reliable in Masdar City does not mean we could obtain such good fidelity in another urban environment. For this reason, it would be interesting to apply the same analysis to a dense urban area where waste heat releases and anthropogenic heat gains would have a significant impact. Finally, a sensitivity analysis on each model parameter would be of interest by demonstrating which parameters have a strong impact on urban temperature and humidity. The sensitivity of annual cooling demand and the peak load would be of particular interest.

Acronyms

BCVTB Building Controls Virtual Test Bed
D² Squared Deviation
DNI Direct Normal Irradiance
DHI Diffuse Horizontal Irradiance
HVAC Heat Ventilation and Air Conditioning
K–S Kolmogorov–Smirnov
MAPE Mean Absolute Percentage Error
RC Resistance and Capacitance
RMSE Root Mean Square Error
RMSH Root Mean Square error of Hellinger
TARP Thermal Analysis Research Program
TEB Town Energy Balance
TMY Typical Meteorological Year
UBL Urban Boundary Layer
UCL Urban Canopy Layer
UHI Urban Heat Island
UWG Urban Weather Generator

Appendix A. Exhaust heat

By exhaust heat, we mean the heat flux traveling from the indoor to the outdoor environment through an air handling unit. Therefore, the computation of exhaust heat consists in estimating the rate required to lower (or raise) the outdoor enthalpy to that of the air exiting the air handling unit:

$$Q_{ex} = \delta_{ex}\dot{m}_{mv}c_p(T_{out} - T_{ex}) \tag{23}$$

$$\widetilde{Q}_{ex} = \delta_{ex}\dot{m}_{mv}L_v(q_{out} - q_{ex}) \tag{24}$$

where $c_p = 1.006 \times 10^3$ J/(kg K) and $L_v = 2.501 \times 10^6$ J/kg are the dry air specific heat capacity and the water latent heat of vaporization, respectively. Using an EnergyPlus model, we can obtain the sensible and latent heat needed to lower the outdoor air enthalpy to the level of the enthalpy of the air rejected by the zones (i.e. $Q_{ex,zones}$ and $\widetilde{Q}_{ex,zones}$, respectively). A zone consists in an indoor air volume we want to keep at a given temperature. Considering that an air handling unit could include sensible and latent energy recovery wheels such as $Q_{recov} = \eta_T Q_{ex,zones}$ and $\widetilde{Q}_{recov} = \eta_q \widetilde{Q}_{ex,zones}$, the exhaust air temperature and humidity can be calculated as:

$$T_{ex} = T_{ex,zones} + \frac{Q_{recov}}{\dot{m}_{mv}c_p} \tag{25}$$

$$q_{ex} = q_{ex,zones} + \frac{\widetilde{Q}_{recov}}{\dot{m}_{mv}L_v} \tag{26}$$

Substituting the exhaust air temperature and humidity defined in Eqs. (25) and (26) into Eqs. (23) and (24), respectively, the sensible and latent heats Q_{ex} and $\widetilde{Q}_{ex}$ going into the urban canyon can be expressed as:

$$Q_{ex} = \delta_{ex}(Q_{ex,zones} - Q_{recov}) \tag{27}$$

$$\widetilde{Q}_{ex} = \delta_{ex}(\widetilde{Q}_{ex,zones} - \widetilde{Q}_{recov}) \tag{28}$$

Appendix B. Masdar wind tower

The Masdar Wind Tower is located 50 m from the Wave Block canyon. This facility provides fresh and humid air between 6:00 am and midnight. It can capture upper-level winds and direct them to the open-air public square at its base. At the top of the steel structure, sensors operate high-level louvers to open in the direction of prevailing winds (and to close in other directions). A polytetrafluoroethylene membrane tube carries the wind downward. More precisely the mist generators inject water droplets which adiabatically cool the air to saturation point. The wind tower combines evaporative cooling and air movement techniques to help moderate perceived air temperatures in the public square at the tower's base (cf. Fig. 20).

The mass flow rate in the wind tower is estimated based on an empirical relation. A wind tunnel experiment was carried out to determine the optimal louver positions for each wind direction [32]. At the same time, the velocity ratio $vr(\widehat{U}_{ubl})$ was measured for each wind direction $\widehat{U}_{ubl}$. To estimate the mass flow rate in the wind tower $\dot{m}_{wt}$, the velocity ratio as seen in Table 7 can be used as following:

$$\dot{m}_{wt} = \rho_{wt}A_{wt}v_r(\widehat{U}_{ubl})U_{ubl} \tag{29}$$

where A_{wt} is the cross-sectional area of in the wind tower tube. The mass flow rate $\dot{m}_{wt}$ in the wind tower was empirically assessed based on the velocity ratio between the wind speed measured in the tube and the one at the entrance of the louvers.

Table 7
Empirical values of the velocity ratio for the wind tower.

$\widehat{U}_{ubl}$	$v_r(\widehat{U}_{ubl})$	$\widehat{U}_{ubl}$	$v_r(\widehat{U}_{ubl})$	$\widehat{U}_{ubl}$	$v_r(\widehat{U}_{ubl})$
0	0.5	130	0.38	260	0.49
10	0.49	140	0.41	270	0.53
20	0.5	150	0.38	280	0.4
30	0.49	160	0.42	290	0.27
40	0.48	170	0.41	300	0.39
50	0.43	180	0.27	310	0.27
60	0.37	190	0.22	320	0.42
70	0.3	200	0.4	330	0.52
80	0.4	210	0.42	340	0.54
90	0.49	220	0.44	350	0.51
100	0.51	230	0.42	360	0.43
110	0.52	240	0.49		
120	0.51	250	0.51		

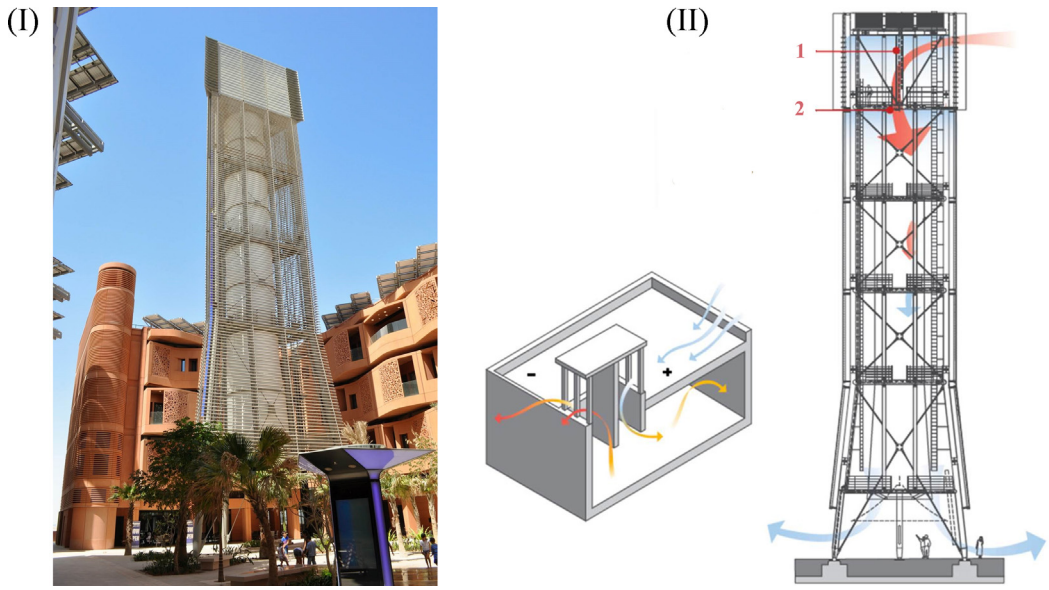

Fig. 20. Masdar Institute wind tower with automatically controllable louvers (1) and mist jets (2).

Referring to the psychrometric chart, the output air temperature T_{wt} was approximated by computing the temperature of moist air at 100 percent relative humidity with enthalpy equal to the input air (at temperature T_{ubl} and specific humidity q_{ubl}). Therefore, the sensible and latent heat fluxes were defined as following:

$$Q_{wt} = \delta_{wt} H_{wt} \dot{m}_{wt} c_p (T_{wt} - T_{urb}) \quad (30)$$

$$\widetilde{Q}_{wt} = \delta_{wt} H_{wt} \dot{m}_{wt} L_v (q_{wt} - q_{urb}) \quad (31)$$

where H_{wt} is equal to one if the wind tower is running at hour h, and zero otherwise.

Appendix C. Supplementary data

Supplementary data associated with this article can be found, in the online version, at http://dx.doi.org/10.1016/j.enbuild.2015.02.047.

References

[1] V. Masson, L. Gomes, G. Pigeon, C. Liousse, V. Pont, J.-P. Lagouarde, J. Voogt, J. Salmond, T.R. Oke, J. Hidalgo, et al., The canopy and aerosol particles interactions in Toulouse urban layer (CAPITOUL) experiment, Meteorol. Atmos. Phys. 102 (3-4) (2008) 135–157.
[2] M.W. Rotach, R. Vogt, C. Bernhofer, E. Batchvarova, A. Christen, A. Clappier, B. Feddersen, S.E. Gryning, G. Martucci, H. Mayer, et al., BUBBLE – an urban boundary layer meteorology project, Theor. Appl. Climatol. 81 (3-4) (2005) 231–261.
[3] Y. Charabi, A. Bakhit, Assessment of the canopy urban heat island of a coastal arid tropical city: the case of Muscat, Oman, Atmos. Res. 101 (1) (2011) 215–227.
[4] H.A. Nasrallah, A.J. Brazel, R.C. Balling, Analysis of the Kuwait City urban heat island, Int. J. Climatol. 10 (4) (1990) 401–405.
[5] E. Jáuregui, A. Tejeda, Urban–rural humidity contrasts in Mexico City, Int. J. Climatol. 17 (2) (1997) 187–196.
[6] V. Masson, A physically-based scheme for the urban energy budget in atmospheric models, Bound.-Layer Meteorol. 94 (3) (2000) 357–397.
[7] A. Martilli, A. Clappier, M.W. Rotach, An urban surface exchange parameterization for mesoscale models, Bound.-Layer Meteorol. 104 (2) (2002) 261–304.
[8] H. Kusaka, F. Kimura, Thermal effects of urban canyon structure on the nocturnal heat island: numerical experiment using a mesoscale model coupled with an urban canopy model, J. Appl. Meteorol. 43 (12) (2004) 1899–1910.
[9] W.A. Friess, K. Rakhshan, T.A. Hendawi, S. Tajerzadeh, Wall insulation measures for residential villas in Dubai: a case study in energy efficiency, Energy Build. 44 (2012) 26–32.
[10] A. Afshari, C. Nikolopoulou, M. Martin, Life-cycle analysis of building retrofits at the urban scale – a case study in United Arab Emirates, Sustainability 6 (1) (2014) 453–473.
[11] B. Bueno, L. Norford, G. Pigeon, R. Britter, Combining a detailed building energy model with a physically-based urban canopy model, Bound.-Layer Meteorol. 140 (3) (2011) 471–489.
[12] D.B. Crawley, L.K. Lawrie, F.C. Winkelmann, W.F. Buhl, Y.J. Huang, C.O. Pedersen, R.K. Strand, R.J. Liesen, D.E. Fisher, M.J. Witte, et al., EnergyPlus: creating a new-generation building energy simulation program, Energy Build. 33 (4) (2001) 319–331.
[13] B. Bueno, L. Norford, G. Pigeon, R. Britter, A resistance–capacitance network model for the analysis of the interactions between the energy performance of buildings and the urban climate, Build. Environ. 54 (2012) 116–125.
[14] B. Bueno, R. Matthias, L. Norford, R. Li, Computationally efficient prediction of canopy level urban air temperature at the neighborhood, Urban Clim. 9 (0) (2014) 35–53.
[15] M. Wetter, Building Control Virtual Testbed – BCVTB, 2009.
[16] US DOE, EnergyPlus engineering reference. The Reference to EnergyPlus Calculations, 2013.
[17] B. Bueno Unzeta, An urban weather generator coupling a building simulation program with an urban canopy model, 2010.
[18] P. Mascart, J. Noilhan, H. Giordani, A modified parameterization of flux-profile relationships in the surface layer using different roughness length values for heat and momentum, Bound.-Layer Meteorol. 72 (4) (1995) 331–344.
[19] C.S.B. Grimmond, T.R. Oke, Aerodynamic properties of urban areas derived from analysis of surface form, J. Appl. Meteorol. 38 (9) (1999) 1262–1292.
[20] G. Walton, TARP – Thermal Analysis Research Program, User Manual, 1984.
[21] B. Bueno Unzeta, Study and Prediction of the Energy Interactions Between buildings and the Urban Climate, Massachusetts Institute of Technology, 2012, Ph.D. thesis.
[22] J. Noilhan, J.-F. Mahfouf, The ISBA land surface parameterization scheme, Glob. Planet. Change 13 (1) (1996) 145–159.
[23] J. Noilhan, S. Planton, A simple parameterization of land surface processes for meteorological models, Mon. Weather. Rev. 117 (3) (1989) 536–549.
[24] D.P. Allen, A frequency domain Hampel filter for blind rejection of sinusoidal interference from electromyograms, J. Neurosci. Methods 177 (2) (2009) 303–310.
[25] W.T.L. Chow, M. Roth, Temporal dynamics of the urban heat island of Singapore, Int. J. Climatol. 26 (15) (2006) 2243–2260.
[26] J.M. Wallace, P.V. Hobbs, Atmospheric science: an introductory survey, vol. 92, Academic Press, 2006.
[27] M.C. McCumber, R.A. Pielke, Simulation of the effects of surface fluxes of heat and moisture in a mesoscale numerical model: 1. Soil layer, J. Geophys. Res.: Oceans (1978–2012) 86 (C10) (1981) 9929–9938.
[28] B.S. Everitt, The Cambridge Dictionary of Statistics, Cambridge, Cambridge, 2002.

[29] EPA, Reducing Urban Heat Islands: Compendium of Strategies Urban Heat Island Basics, 2009, available at http://www.epa.gov/hiri/resources/compendium.htm
[30] T. Ihara, Y. Genchi, T. Sato, K. Yamaguchi, Y. Endo, City-block-scale sensitivity of electricity consumption to air temperature and air humidity in business districts of Tokyo, japan, Energy 33 (11) (2008) 1634–1645.
[31] Y. Rubner, C. Tomasi, L.J. Guibas, The earth mover's distance as a metric for image retrieval, Int. J. Comput. Vis. 40 (2) (2000) 99–121.
[32] S. Carmichael, D. Philips, A. Belanger, A. Davies, MIST – wind tower controls louver operation & mist release. Technical report, Rowan 42 Williams Davies & Irwin Inc., Canada, August 2009.